Electronic Supplementary Material (ESI) for Catalysis Science & Technology.


# Bismuth single atoms supported $CeO_2$ nanosheets for oxidation resistant photothermal reverse water gas shift reaction

Xiaoxiao Kang,‡[a] Dachao Yuan,‡[b] Zhiqi Yi,‡[a] Chenyang Yu,[a] Xiaoxian Yuan,*[a] Baolai Liang,[a] Xingyuan San,[a] Linjie Gao,[a] Shufang Wang,[a] Yaguang Li*[a]

[a] Hebei Key Lab of Optic-electronic Information and Materials, The College of Physics Science and Technology, Institute of Life Science and Green Development, Hebei University, Baoding, 071002, China.

[b] College of Mechanical and Electrical Engineering, Hebei Agricultural University, Baoding 071001, P. R. China

Correspondence and requests for materials should be addressed to X.X. Yuan (yxx@hbu.edu.cn), Y.G. Li (liyaguang@hbu.edu.cn)

‡These authors contributed equally to this work.

# Experimental section

## The homemade $Ti_2O_3$ based device

The SP-0707AS magnetron sputtering was used to deposit $Ti_2O_3$ film, which had the vacuum pressure lower than $7.0\times10^{-3}$ Pa, and a 4 axis rotation system to rotate bases. $Ti_2O_3$ and Cu were used as targets; the working gas was Ar with 99.99 % purity. For the synthesis of $Ti_2O_3$/Cu based device, the deposition of Cu substrate and $Ti_2O_3$ film on reaction tube was first using glow-discharge to clean glass tube, then depositing Cu layer by Cu target and $Ti_2O_3$ film by $Ti_2O_3$ target orderly, finally taking out the sample after passive cooling. Specific parameters: the power was 5 KW, the sputtering pressure was $9\times10^{-2}$ Pa, the bias voltage was 150 V, the sputtering temperature was 70 °C, the sputtering time for Cu layer, $Ti_2O_3$ film was 12 min, 6 min, respectively. The followed glass vacuum layer was provided by Hebei scientist research experimental and equipment trade Co., Ltd. with $1\times10^{-3}$ Pa of pressure.

## Characterization

The prepared samples were studied by the powder X-ray diffraction (XRD), which was performed on a Bede D1 system operated at 40 kV and 40 mA with Cu Kα radiation (λ= 1.5406 Å). Raman spectra were recorded on a HORIBA Raman spectrometer, with an excitation laser wavelength of 532 nm. The Xray photoelectron spectra (XPS) were recorded on a Thermo ESCALAB-250 spectrometer with a monochromatic Al Kα radiation source (1486.6 eV). The binding energies determined by XPS were corrected

by referring the adventitious carbon peak (284.8 eV) for each sample. The scanning electron microscopy (SEM) images were tested with the FEI Nova NanoSEM450 (Czech Republic). Transmission electron microscopy (TEM, JEM-2100 Plus) and Aberration-corrected Transmission electron microscopy (AC-TEM, JEM-ARM 200) were used to identify the morphology, crystal structure of the nanostructures. The BET surface areas were obtained using a Micromeritics Tristar 3020 system. Hydrogen temperature-programmed reduction ($H_2$-TPR) was carried out using an online gas chromatograph (GC-7090A) equipped with a TCD detector. In a typical process, 50 mg of catalysts was placed in a quartz tube (6 mm ID). Subsequently, TPR was performed by heating the samples from room temperature to 600 °C at the heating rate of 5 °C /min, in the presence of a 10% $H_2$/Ar mixture (50 ml/min) flowing.

The CO production rate V (mmol $g^{-1}$ $h^{-1}$) was calculated as following equations:

$$V\ (\text{mmol}\ g^{-1}\ h^{-1}) = (v*[CO]_{outlet}/24.5)/m \quad (1)$$

v was the feed gas rate (ml $h^{-1}$), $[CO]_{outlet}$ was CO concentration which can be obtained by GC, m was the weight of catalysts.

The CO production rate from solar-heating catalysis system was calculated as following equations:

$$s\ (\text{mmol}\ m^{-2}\ h^{-1}) = (v*[CO]_{outlet}/24.5)/S \quad (2)$$

S was the irradiation area.

The selectivity was calculated as following equations:

$$\text{CO Selectivity} = [CO]_{outlet}/([CO]_{outlet}+[CH_4]_{outlet})*100\% \quad (3)$$

The conversion of $CO_2$ was calculated as following equations:

$CO_2$ Conversion = $([CO]_{outlet} + [CH_4]_{outlet})/[CO_2]_{inlet} * 100\%$ (4)

The TOF was calculated as follows:

TOF ($min^{-1}$) = $V/(60 * Bi^*_a)$ (6)

$Bi^*_a$ was the mole quantity of bismuth in $BiO_x/CeO_2$.

The ex-situ Bi $L_3$-edge extended X-ray absorption fine structure (EXAFS) data were collected on the beamline at Shanghai Synchrotron Radiation Facility (SSRF). All samples were prepared by placing a small amount of homogenized (via agate mortar and pestle) powder on 3 M tape. We used IFEFFIT software to calibrate the energy scale, correct the background signal and normalize the intensity. The spectra were normalized with respect to the edge height after subtracting the pre-edge and post-edge backgrounds using Athena software. To extract the EXAFS oscillations, the background was removed in k-space using a five-domain cubic spline. The resulting k-space data were then Fourier transformed.

**First-principles calculations**

We have employed the Vienna Ab Initio Package (VASP) to perform all the density functional theory (DFT) calculations within the generalized gradient approximation (GGA) using the PBE formulation[1-3]. We have chosen the projected augmented wave (PAW) potentials to describe the ionic cores and take valence electrons into account using a plane wave basis set with a kinetic energy cutoff of 400 eV. Partial occupancies of the Kohn−Sham orbitals were allowed using the Gaussian smearing method and a width of 0.05 eV. The electronic energy was considered self-consistent when the energy change was smaller than $10^{-5}$ eV. A geometry optimization was considered convergent

when the force change was smaller than 0.02 eV/Å. Grimme's DFT-D3 methodology was used to describe the dispersion interactions[4].

We used $CeO_2$ (111) facet as the model. The equilibrium lattice constant of hexagonal $CeO_2$ unit cell separated by a vacuum layer in the depth of 30 Å was optimized. We then used it to construct a $CeO_2$ model with *p* (4x4x1) periodicity in the x, y, z directions by vacuum depth of 30 Å in order to separate the surface slab from its periodic duplicates. During structural optimizations, the gamma point in the Brillouin zone was used for k-point sampling, and all atoms were allowed to relax.

The adsorption energy ($E_{ads}$) of adsorbate A was defined as

$$E_{ads} = E_{A/surf} - E_{surf} - E_{A(g)}$$

where $E_{A/surf}$, $E_{surf}$ and $E_{A(g)}$ are the energy of adsorbate A adsorbed on the surface, the energy of clean surface, and the energy of isolated A molecule in a cubic periodic box with a side length of 20 Å. K-spacing was set to 0.4 for all structure to allow the smallest spacing between k-points in units of 0.4 $Å^{-1}$.

**Table S1.** EXAFS fitting parameters of $BiO_x/CeO_2$ extracted from the Bi $L_3$-edge

| sample | Path | CN | $\sigma^2(10^{-3}$ Å$^2)$ | R | $\Delta E_0$(eV) |
|---|---|---|---|---|---|
| $BiO_x/CeO_2$ | Bi-O | 7 | 6.2±0.4 | 1.48±0.03 | 7.2 |

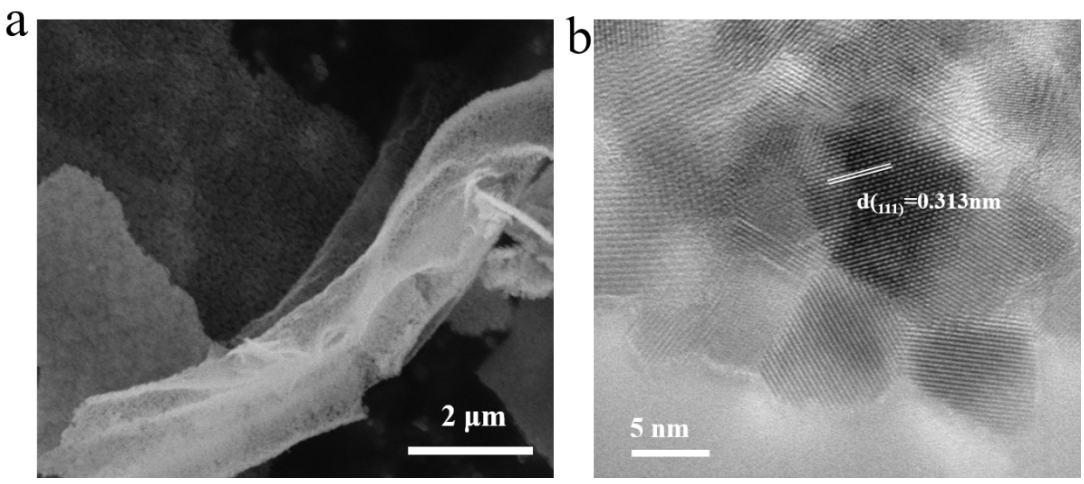


**Fig. S1** (a, b) SEM and HRTEM image of $BiO_x/CeO_2$.

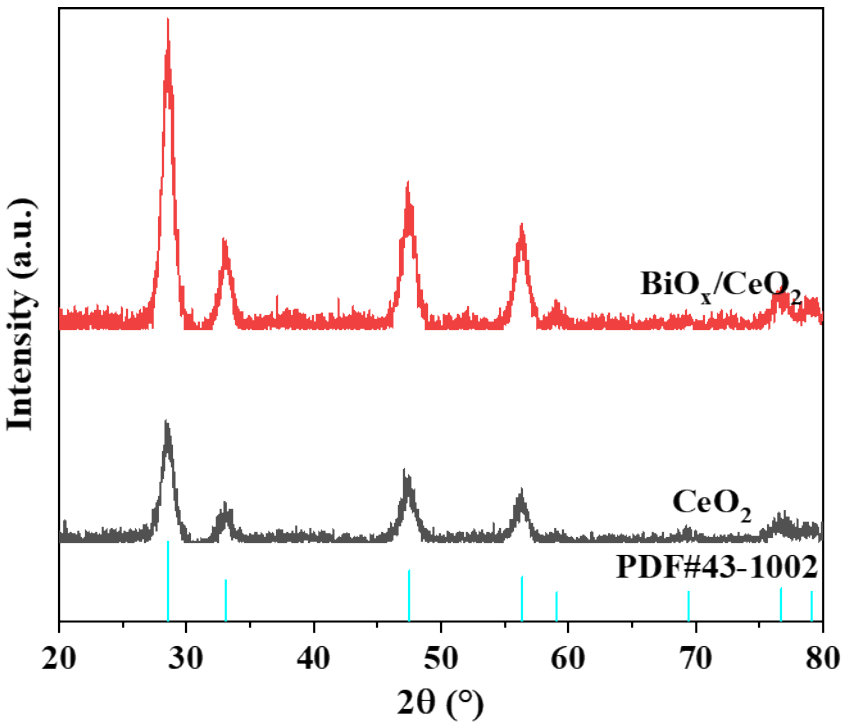


**Fig. S2** XRD pattern of $BiO_x/CeO_2$ and $CeO_2$.

The XRD pattern of $BiO_x/CeO_2$ only showed the peaks similar to cubic $CeO_2$ crystal phase, and the peaks moved towards a high angle a little because the ionic radius of $Ce^{4+}$is larger than $Bi^{3+}$ ($Ce^{4+}$:1.07 Å, $Bi^{3+}$:0.96 Å), indicating the highly dispersed bismuth might be doped in $CeO_2$ lattice.

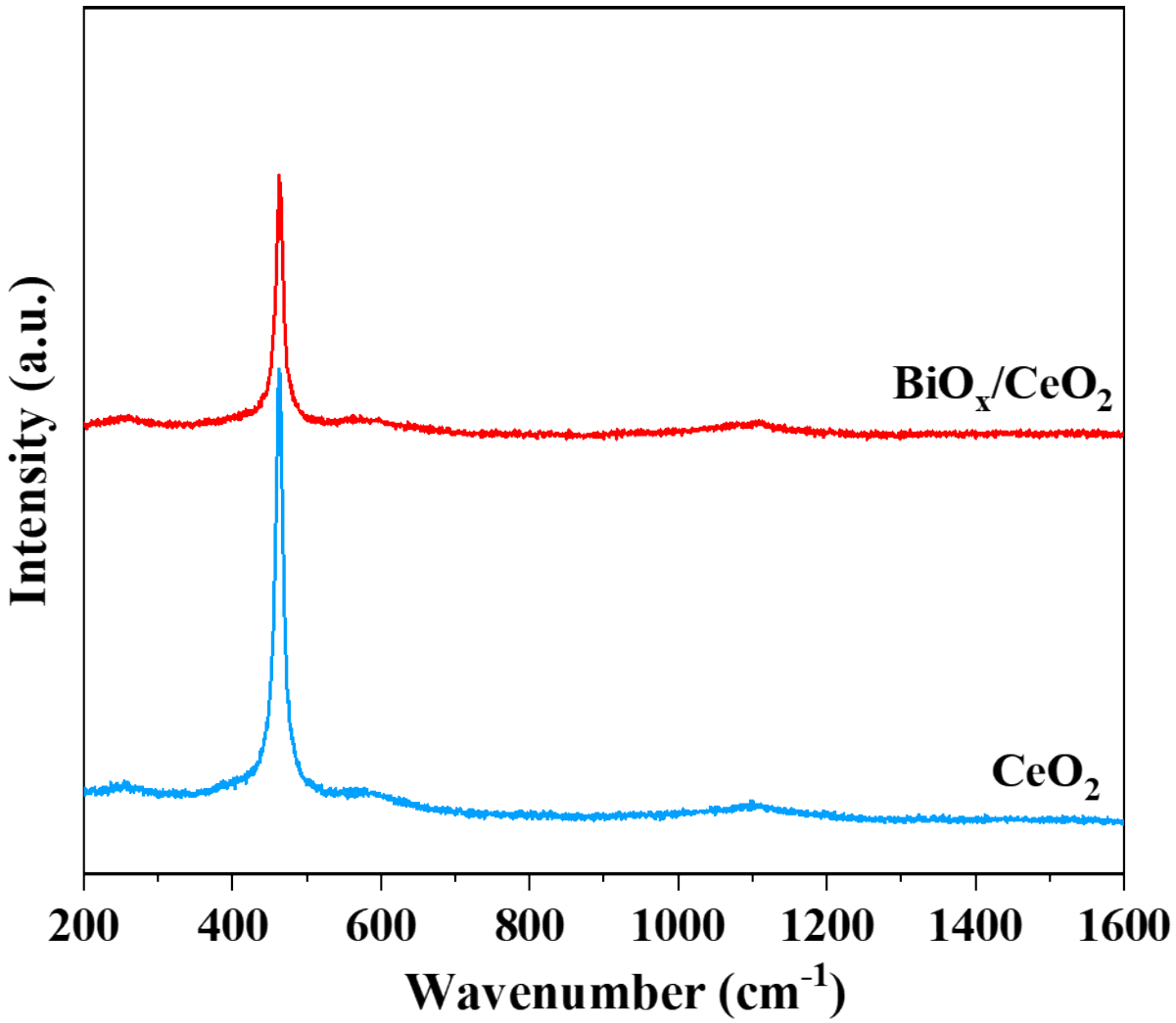


**Fig. S3** Raman spectrum of $BiO_x/CeO_2$ and $CeO_2$.

For the $CeO_2$ support, four peaks were observed in spectra: a strong peak at 463 $cm^{-1}$ and three weak peaks at 463, 570 and 1114 $cm^{-1}$, which correspond to fluorite $F_{2g}$ mode, second order transverse acoustic (2TA) mode, defect induced (D) and second order longitudinal optical (2LO) mode, respectively[5, 6]. For the $BiO_x/CeO_2$ sample, the same characteristic peaks were shown in $BiO_x/CeO_2$ except for a slight to lower wavenumber, which might be caused by the introduction of Bi atoms.

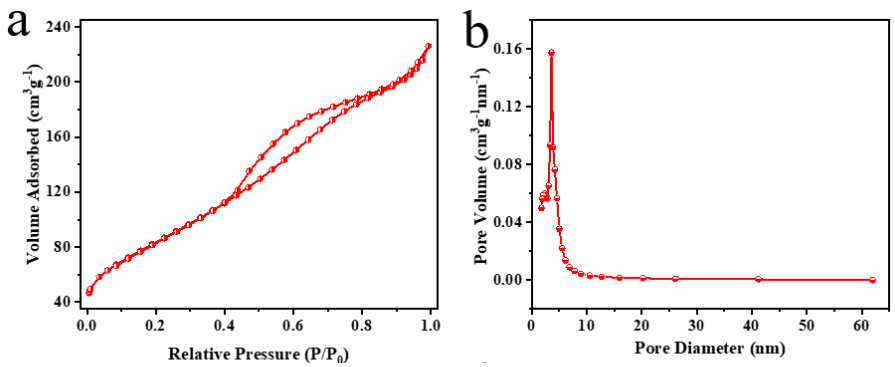


**Fig. S4** (a) BET plot of $BiO_x/CeO_2$ and (b)corresponding pore distribution.

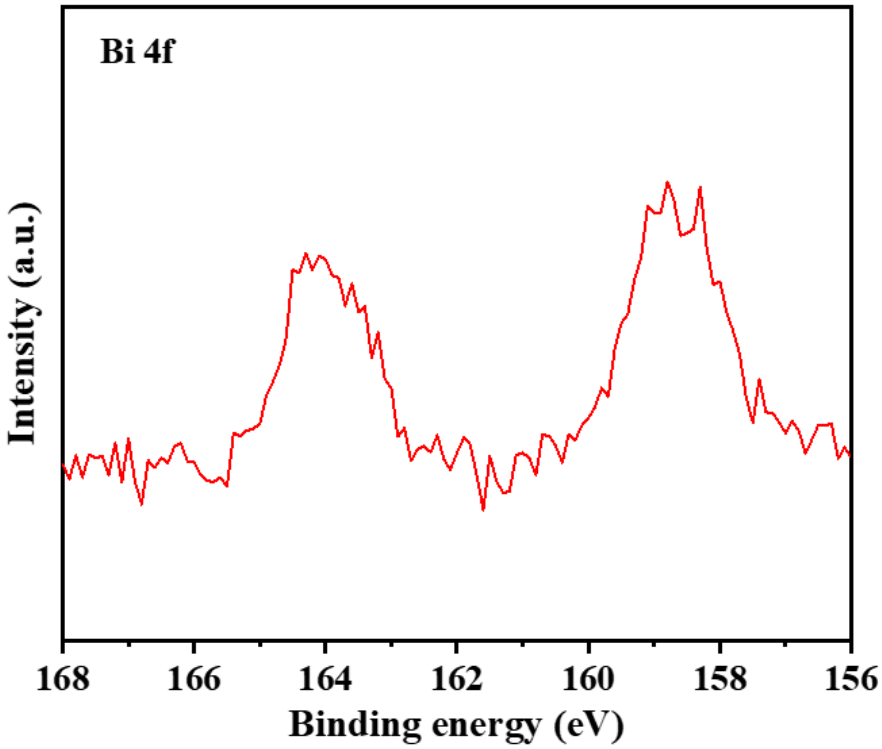


**Fig. S5** Bi 4f XPS peaks of $BiO_x/CeO_2$.

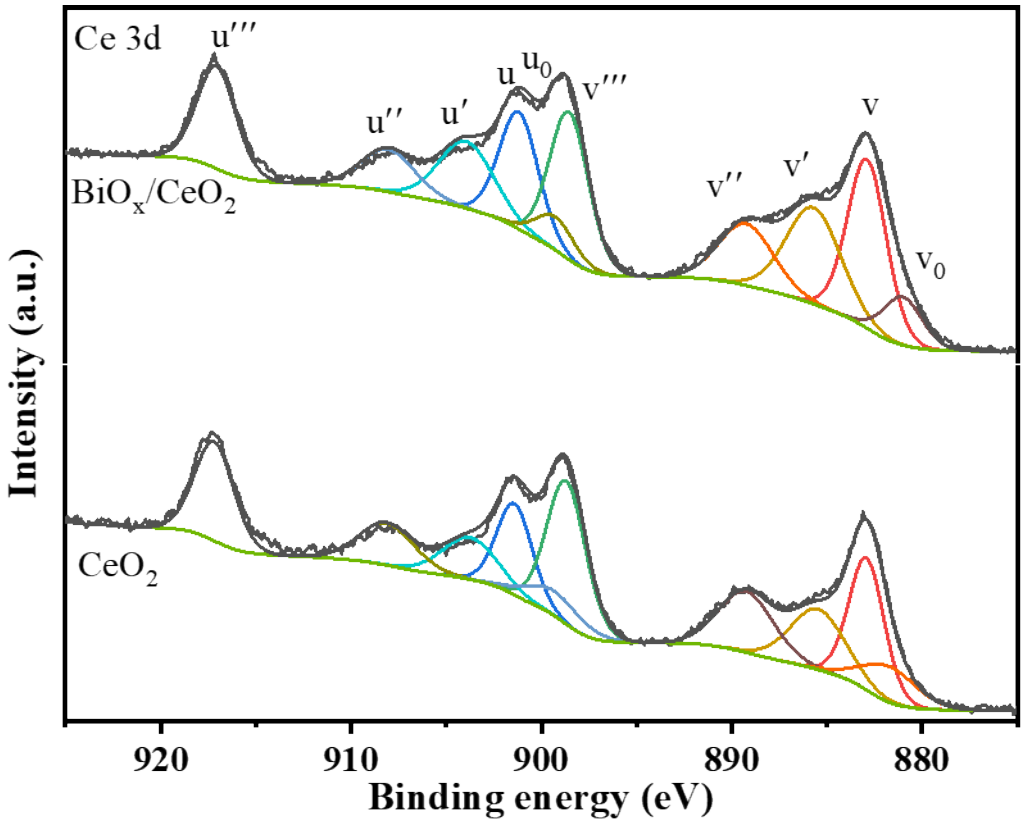


**Fig. S6** Ce 3d XPS peaks of $BiO_x/CeO_2$ and $CeO_2$.

The XPS spectra of the Ce 3d core level can be resolved into ten groups[7, 8]. The five main $3d_{5/2}$ features are denoted as $v_0$ (881.0 eV), v (882.9 eV), v' (885.7 eV), v'' (889.2 eV) and v''' (898.5 eV) components, and the five $3d_{3/2}$ features are assigned to $u_0$ (899.3 eV), u (901.2 eV), u' (903.9 eV), u'' (908.1 eV) and u''' (917.0 eV), respectively[8]. The amount of surface $Ce^{3+}$ ion can be determined by $Ce^{3+} = Ce^{3+}/(Ce^{3+} + Ce^{4+})$, where $Ce^{3+} = v_0 + v' + u_0 + u'$ and $Ce^{4+} = v + v'' + v''' + u + u'' + u'''$. The $Ce^{3+}$ concentration can be correlated to the oxygen vacancies on the ceria surface, and $BiO_x/CeO_2$ and $CeO_2$ almost $Ce^{3+}$ concentration (32.12% vs 31.26%).

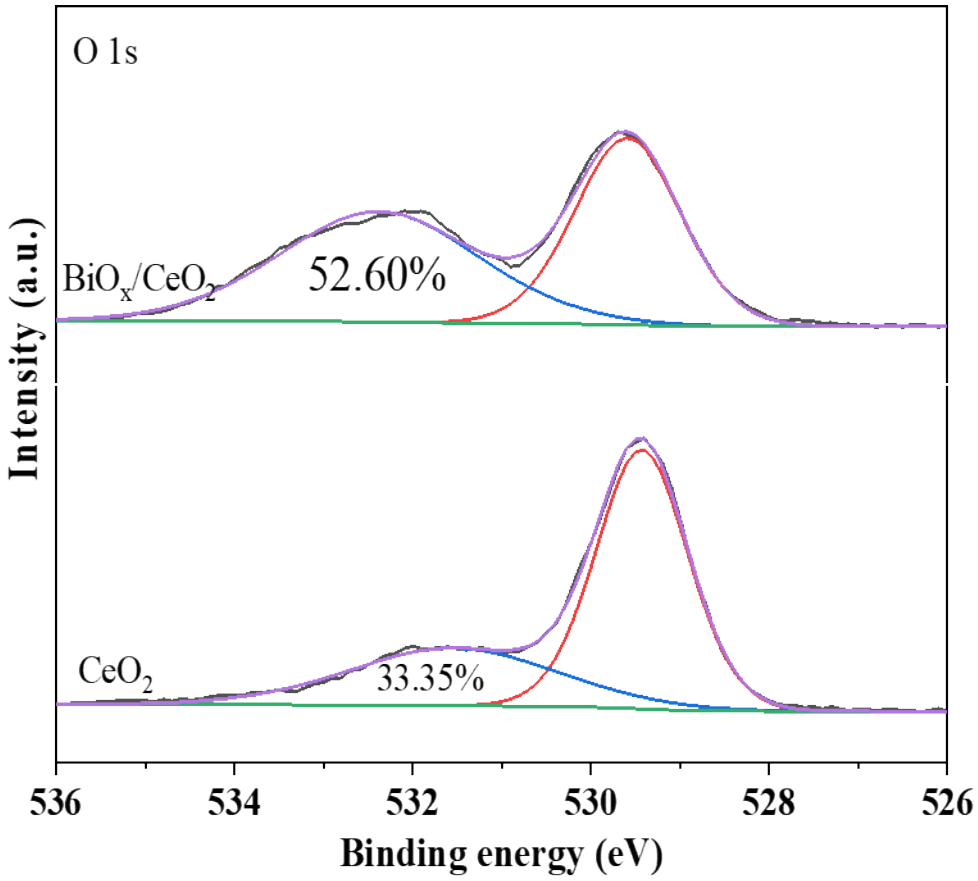


Fig. S7 The O 1s XPS peaks of $BiO_x/CeO_2$ and $CeO_2$.

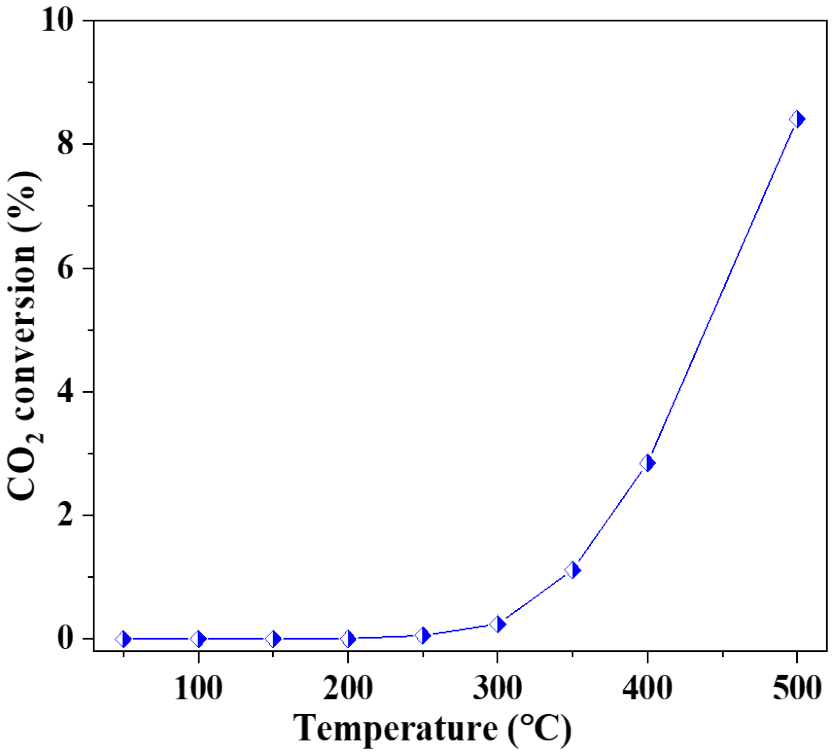


Fig. S8 The thermal catalysis $CO_2$ conversion rate by $BiO_x/CeO_2$ catalysts under different temperature.

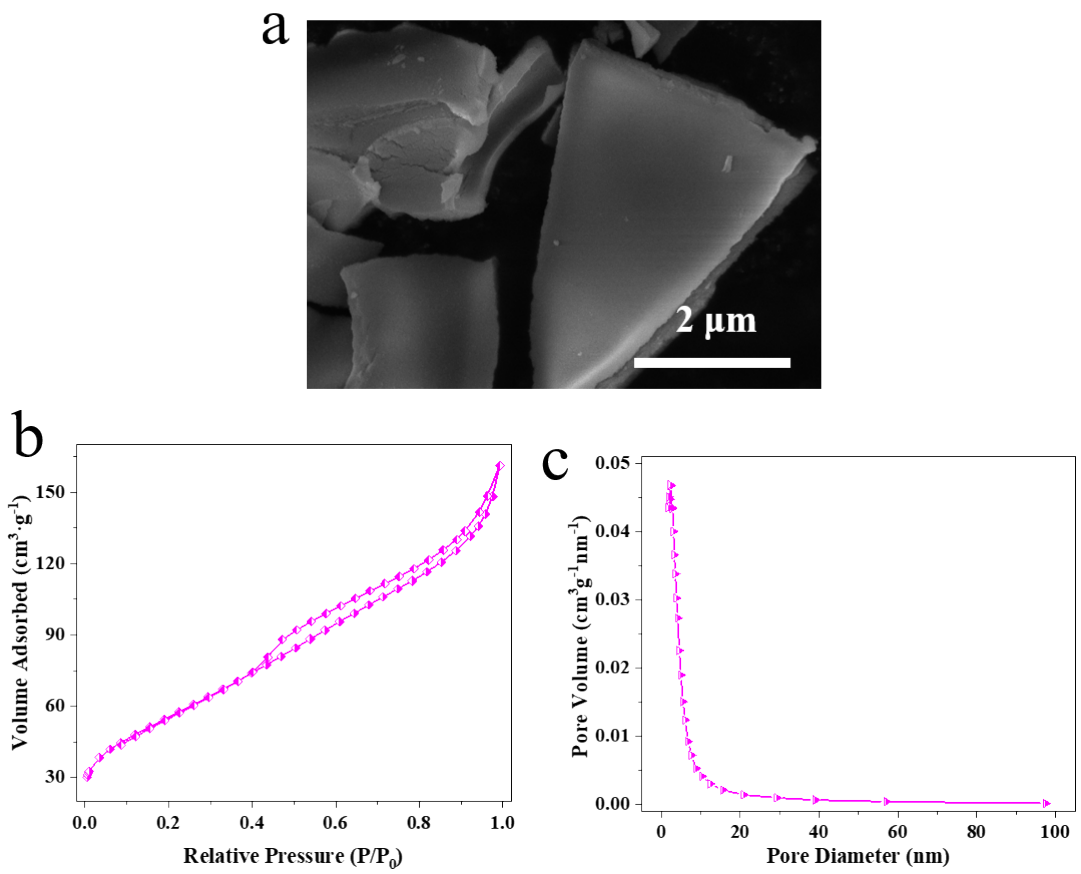


**Fig. S9** (a) SEM image of $CeO_2$. (b) BET plot of pure $CeO_2$ and (c) corresponding pore distribution.

The specific surface area of $CeO_2$ nanosheet is only 202.45 $m^2$ $g^{-1}$ with a pore size of 4.8 nm (Fig. S9 b, c).

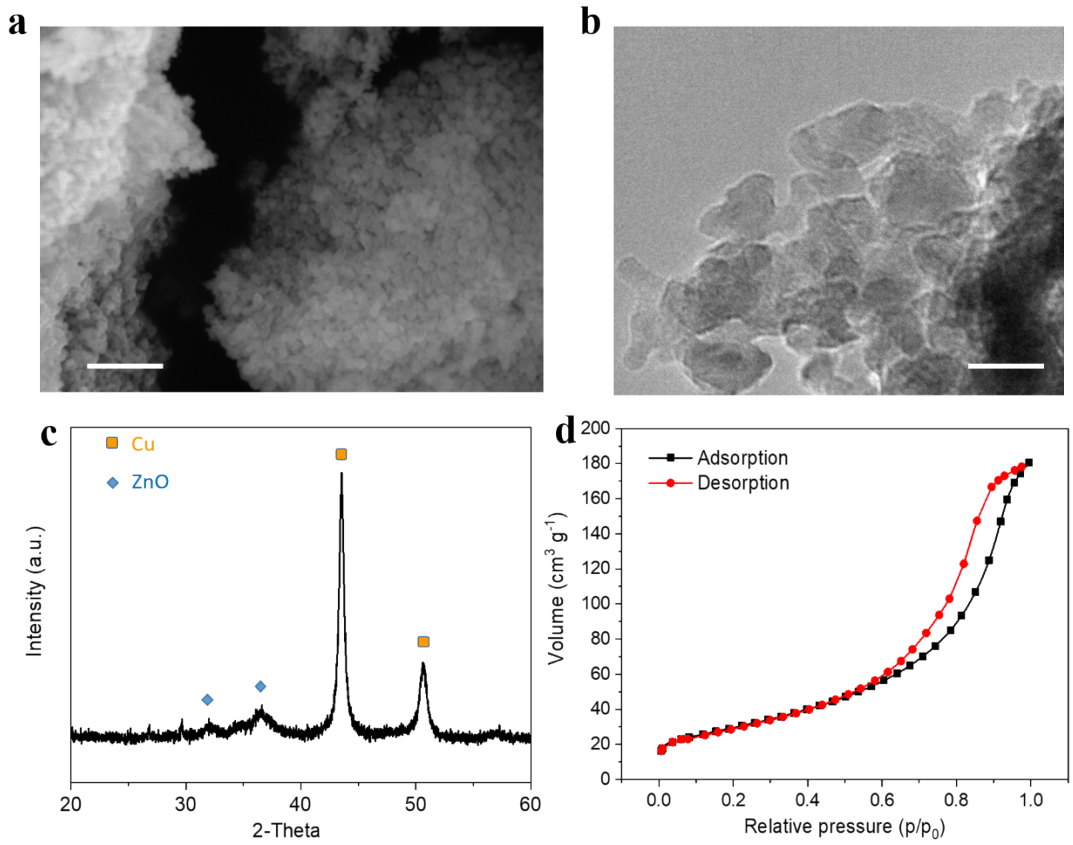


**Fig. S10** SEM image (a), TEM image (b), XRD pattern (c), nitrogen adsorption and desorption isotherm (d) of commercial $CuO_x/ZnO/Al_2O_3$.

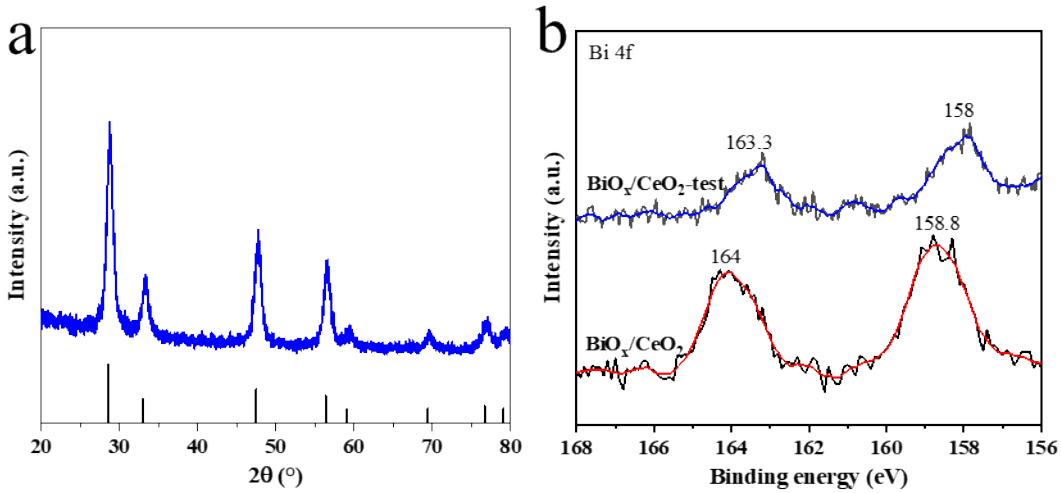


**Fig. S11** (a) XRD pattern of $BiO_x/CeO_2$ after stability test (b) The Bi 4f XPS peaks of $BiO_x/CeO_2$ before and after stability test.

The Bi 4f XPS peaks of $BiO_x/CeO_2$ changed about 0.8 eV before and after test, but the oxidation state of Bi is 3+[9, 10].

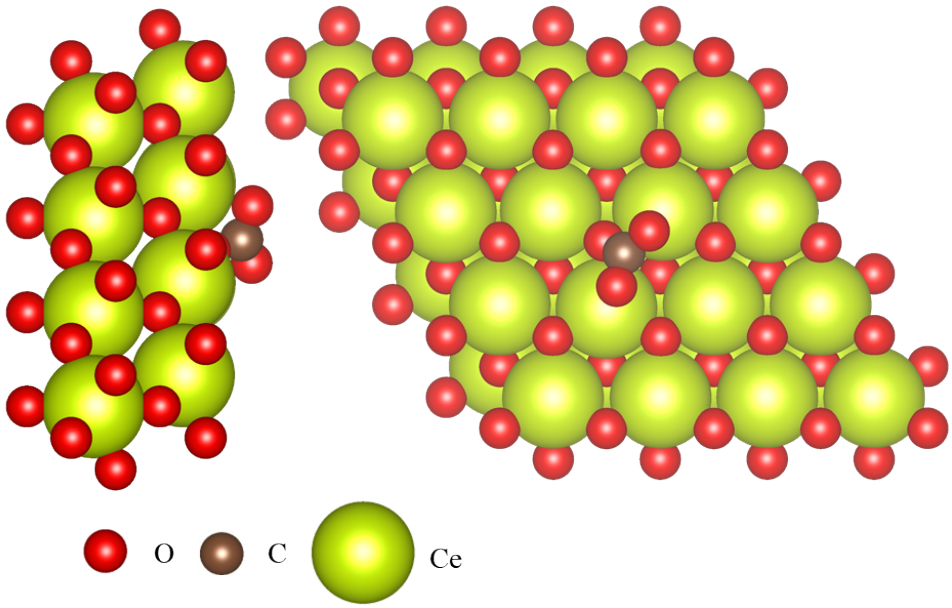


**Fig. S12** Side and top views of $CO_2$ adsorption over $CeO_2$ (111).

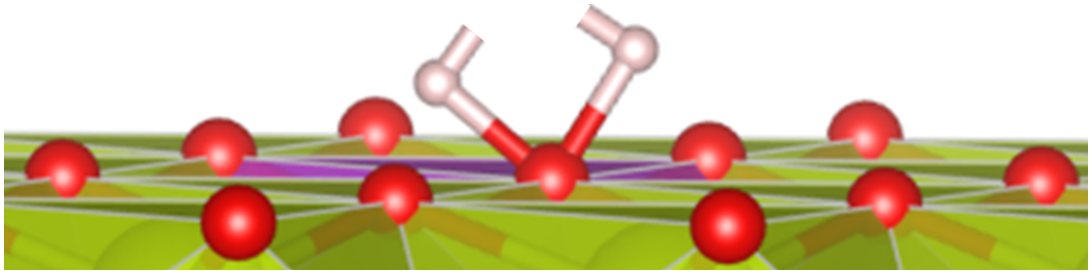

Fig. S13 The spontaneous reaction of $H_2$ with catalysts near $BiO_x/CeO_2$.

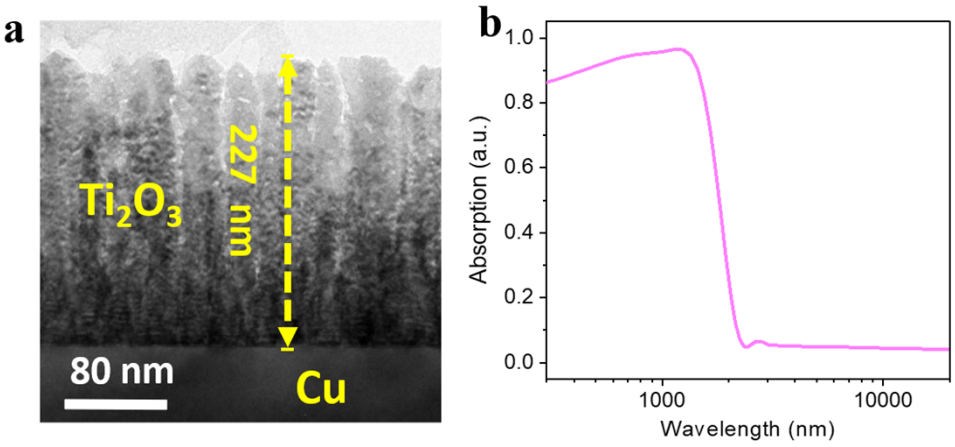


**Fig. S14** (a, b) TEM image and normalized light absorption spectrum of $Ti_2O_3$/Cu.

Fig. S15 The setup image for photothermal $CO_2$ reduction test.

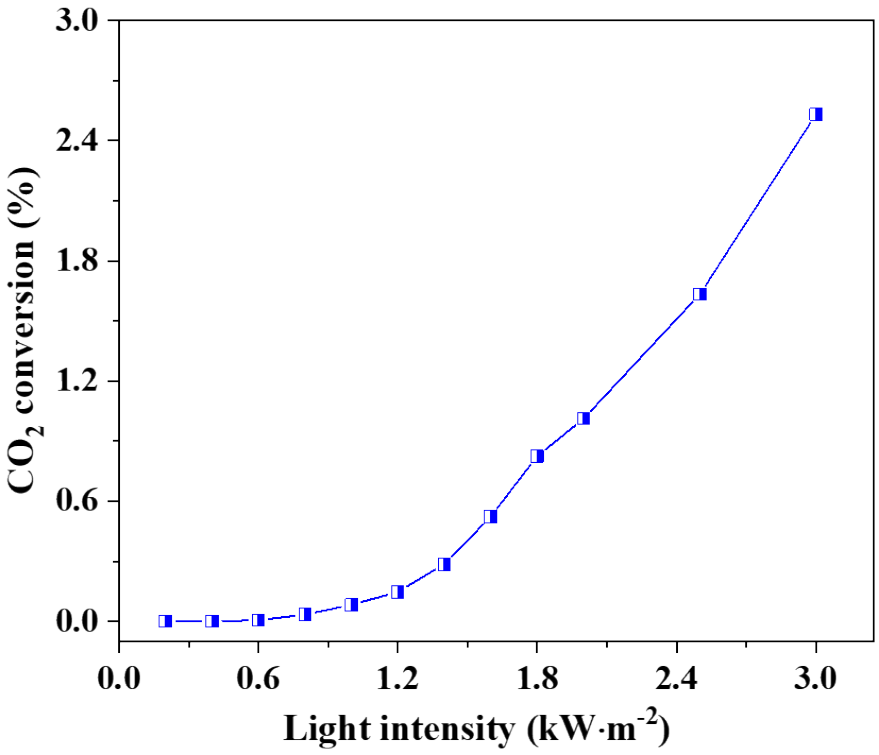


Fig. S16 The photothermal catalysis $CO_2$ conversion rate by $BiO_x/CeO_2$ under different light illumination.

**Reference**

[1] G. Kresse, J. Furthmüller, Efficiency of ab-initio total energy calculations for metals and semiconductors using a plane-wave basis set, Computational Materials Science, 6 (1996) 15-50.

[2] G. Kresse, J. Furthmüller, Efficient iterative schemes for ab initio total-energy calculations using a plane-wave basis set, Physical Review B, 54 (1996) 11169-11186.

[3] J.P. Perdew, K. Burke, M. Ernzerhof, Generalized Gradient Approximation Made Simple, Physical Review Letters, 77 (1996) 3865-3868.

[4] S. Grimme, J. Antony, S. Ehrlich, H. Krieg, A consistent and accurate ab initio parametrization of density functional dispersion correction (DFT-D) for the 94 elements H-Pu, The Journal of Chemical Physics, 132 (2010) 154104.

[5] Q. Dai, H. Huang, Y. Zhu, W. Deng, S. Bai, X. Wang, G. Lu, Catalysis oxidation of 1,2-dichloroethane and ethyl acetate over ceria nanocrystals with well-defined crystal planes, Applied Catalysis B: Environmental, 117-118 (2012) 360-368.

[6] Z. Hu, X. Liu, D. Meng, Y. Guo, Y. Guo, G. Lu, Effect of Ceria Crystal Plane on the Physicochemical and Catalytic Properties of Pd/Ceria for CO and Propane Oxidation, ACS Catalysis, 6 (2016) 2265-2279.

[7] L.-H. Chang, N. Sasirekha, Y.-W. Chen, W.-J. Wang, Preferential Oxidation of CO in $H_2$ Stream over Au/$MnO_2$−$CeO_2$ Catalysts, Industrial & Engineering Chemistry Research, 45 (2006) 4927-4935.

[8] M. Romeo, K. Bak, J. El Fallah, F. Le Normand, L. Hilaire, XPS Study of the reduction of cerium dioxide, Surface and Interface Analysis, 20 (1993) 508-512.

[9] J. Medina-Ramos, J.L. DiMeglio, J. Rosenthal, Efficient Reduction of $CO_2$ to CO with High Current Density Using in Situ or ex Situ Prepared Bi-Based Materials, Journal of the American Chemical Society, 136 (2014) 8361-8367.

[10] Q. Hao, R. Wang, H. Lu, C.a. Xie, W. Ao, D. Chen, C. Ma, W. Yao, Y. Zhu, One-pot synthesis of C/Bi/$Bi_2O_3$ composite with enhanced photocatalytic activity, Applied Catalysis B: Environmental, 219 (2017) 63-72.